



HAL
open science

Comparison of 2D thermal diffusion approximations with experimental data

Lucas Furlan Rufino da Silva, Stéphane Victor, Andrzej Kusiak, Jean-Luc Battaglia

► **To cite this version:**

Lucas Furlan Rufino da Silva, Stéphane Victor, Andrzej Kusiak, Jean-Luc Battaglia. Comparison of 2D thermal diffusion approximations with experimental data. 12th IFAC Conference on Fractional Differentiation and its Applications ICFDA 2024, Jul 2024, Bordeaux (France), France. pp.209-214, 10.1016/j.ifacol.2024.08.191 . hal-04716229

HAL Id: hal-04716229

<https://hal.science/hal-04716229v1>

Submitted on 1 Oct 2024

HAL is a multi-disciplinary open access archive for the deposit and dissemination of scientific research documents, whether they are published or not. The documents may come from teaching and research institutions in France or abroad, or from public or private research centers.

L'archive ouverte pluridisciplinaire **HAL**, est destinée au dépôt et à la diffusion de documents scientifiques de niveau recherche, publiés ou non, émanant des établissements d'enseignement et de recherche français ou étrangers, des laboratoires publics ou privés.



Distributed under a Creative Commons Attribution - NonCommercial - NoDerivatives 4.0 International License

Comparison of 2D thermal diffusion approximations with experimental data

Lucas Furlan Rufino da Silva,^{*,**} Stéphane Victor,^{*}
 Andrzej Kusiak,^{**} Jean-Luc Battaglia^{**}

^{*} Univ. Bordeaux, CNRS, Bordeaux INP, IMS, UMR 5218, F-33400
 Talence, France (e-mail: firstname.name@ims-bordeaux.fr).

^{**} Univ. Bordeaux, CNRS, Bordeaux INP, IMS, UMR 5295, F-33400
 Talence, France (e-mail: firstname.name@u-bordeaux.fr).

Abstract: The European Space agency is highly interested in a full atmospheric reentry from low Earth orbit conditions using an automatic lifting body. In this respect, a numerical method is performed to estimate the heat transfer conditions at the rear surface of a stainless steel material through solving the heat equation. The proposed models should be easily invertible in order to reconstruct the heat flux. The present study presents the analytical modeling of a 2D thermal diffusion which will be compared to different approximations: Taylor approximation, Padé approximation and finite difference method. A benchmark is developed and the temperature output measurements are compared with the proposed approximations.

Copyright © 2024 The Authors. This is an open access article under the CC BY-NC-ND license (<https://creativecommons.org/licenses/by-nc-nd/4.0/>)

Keywords: Heat equation; heat transfer; system, modeling; thermal system; system identification; thermocouple characterization

1. INTRODUCTION

Thermal modeling of systems is of particular interest in applications where temperature might be critical. This includes air conditioning, industrial refrigeration, electronic device cooling, biological tissue heat losses etc. The complexity of heat transfer usually implies the use of finite element methods to solve the heat equation in a chosen region of space. However, finite element models tend to be complex to calculate and in many cases a simpler model that only takes into account temperatures around particular points of interest are precise enough.

Thermal modeling is usually used in the domain of power electronics (Künzi (2015)), building simulation (Parnis (2012); Danza et al. (2016)), human heat losses (Ismail et al. (2018)), machining and high speed machining or even atmosphere reentry. RC circuit models are present in other similar applications, such as the measurement of bio-impedances (Chinen et al. (2015)) or lithium-ion battery models (Zhang et al. (2017)). In most of these applications, the input is assumed a low frequency signal. In order to widen the frequency range and especially in high frequency, the thermal two-port network was introduced in (Maillet et al. (2000)) and such a model is directly derived from the heat equation. Such a thermal modeling have been used to model heat transfers in lungs (Duhé et al. (2022)).

In aerospace industry, the atmospheric reentry of an object from outer space is a succession of complex phenomena with a large variation of the flow properties. In these circumstances, the prediction of the heat flux is a very challenging issue (Anderson (1989); Kemp and Riddell (1957)). Flight data is a crucial key for most engineering departments, for instance temperature and heat flux in the

fuselage external surface. However its acquisition during reentry is extremely complicated (Pizzarelli et al., 2019).

First, the heat shield should not be severely pierced with holes and other stress concentration points for sensor fixation. Besides, the high temperature and pressure conditions could be so extreme that no device would work.

In real applications, thermocouples are positioned inside the fuselage in such a way it will not be in direct contact with the atmosphere, or in regions with a less severe environment. In this configuration, if one is interested in the temperature or heat flux in the outside surface, it is necessary to know how the heat transfer occurs in the fuselage/sensor. Denoting q^{-1} as the delay operator, let $G_\varphi(q^{-1})$ be the discrete transfer function that describes the measured temperature $T(t)$ given a heat flux on the outside surface $\phi(t)$ (see Fig. 1).

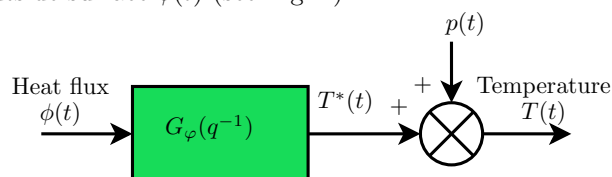


Fig. 1. Thermal system

If the form of $G_\varphi(q^{-1})$ is known, then an easy inversion could be done and using the acquired temperature data, it is possible to return to the heat flux $\phi(t)$ of interest.

The contributions are, firstly, to develop an accurate analytical expression of the thermal system $G_\varphi(s)$. Then, a benchmark is developed for input signal generation via a Labview interface. The main aim of the study is to verify if the approximated methods are sufficiently precise to fit the measured temperature.

The structure of this paper is as follows. Section 2 recalls the analytical modeling of heat transfers by solving the heat equation. Then, Section 3 proposes some numerical approximations of the 2D heat transfer modeling. Section 4 gives a description of the benchmark and compares the approximations with the experimental data. Finally, Section 5 will provide conclusions and prospects.

2. 2D HEAT TRANSFER MODELING

2.1 Time domain approach

Assuming cylindrical coordinates, with x being the linear coordinate, a two-dimensional model of the heat transfer will be studied, as shown in Figure 2. Since the system is cylindrical, the heat transfer can be approximated as axisymmetric.

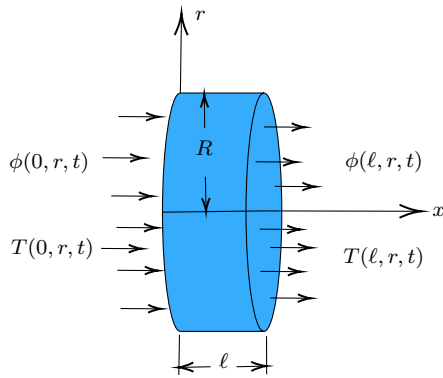


Fig. 2. Heat transfer in 2D

The heat equation in 2D is expressed by

$$\lambda_r \frac{\partial^2 T}{\partial r^2} + \lambda_r \frac{1}{r} \frac{\partial T}{\partial r} + \lambda_x \frac{\partial^2 T}{\partial x^2} = \rho c_p \frac{\partial T}{\partial t}, \quad (1)$$

where $T(x, r, t)$ is the temperature, ρ the material density, c_p the specific heat, λ_r and λ_x the conductivity according to r and x respectively. Let us denote $\phi(x, r, t)$ as the heat flux that propagates in x and r directions (Fig. 2).

When it comes to the boundary conditions, it will be considered that the heat flux applied to the front side of the material (at $x = 0$), is known as a function of time $\phi(0, t)$. Furthermore, a natural convection is considered in the rear side (defined at $x = \ell$), which means that the heat flux will be proportional to the temperature difference between the surface and the ambient temperatures, given by a heat transfer coefficient h_x . A natural convection is also considered in the external cylindrical surface $r = R$, with a coefficient h_x . Besides, there is no heat transfer in the middle $r = 0$ due to its symmetry.

For simplicity sake, let us assume that the initial temperature and the ambient temperature are equal to 0. The boundary conditions are then defined as:

$$-\lambda_x \frac{\partial T}{\partial x} = \phi(0, r, t) \quad \text{for } x = 0, r \leq R_0, \quad (2)$$

$$-\lambda_x \frac{\partial T}{\partial x} + h_x T(\ell, r, t) = 0 \quad \text{for } x = \ell, \quad (3)$$

$$-\lambda_r \frac{\partial T}{\partial r} = 0 \quad \text{for } r = 0, \quad (4)$$

$$-\lambda_r \frac{\partial T}{\partial r} + h_r T = 0 \quad \text{for } r = R. \quad (5)$$

2.2 Frequency domain approach

Applying the Laplace transform to eq. (1), with the boundary conditions (2)-(5), one obtains the solution in the frequency domain, s being the Laplace variable:

$$\frac{\lambda_r}{\lambda_x} \frac{\partial^2 \theta}{\partial r^2} + \frac{\lambda_r}{\lambda_x} \frac{1}{r} \frac{\partial \theta}{\partial r} + \frac{\partial^2 \theta}{\partial x^2} = \frac{s}{a_x} \theta,$$

where $a_x = \lambda_x / c_p \rho$ is the thermal diffusivity in the x direction. First, it will be assumed that the solution θ is separable in two parts, one that only depends in r and another that only depends in x and s , namely:

$$\theta(x, r, s) = \tau(x, s) \psi(r).$$

Substituting it in the heat equation, it then comes

$$\frac{\lambda_r}{\lambda_x} \frac{\partial^2 \psi(r)}{\partial r^2} \frac{1}{\psi(r)} + \frac{\lambda_r}{\lambda_x} \frac{\partial \psi(r)}{\partial r} \frac{1}{r} \frac{1}{\psi(r)} = \frac{1}{\tau} \frac{s}{a_x} \tau(x, s) - \frac{\partial^2 \tau(x, s)}{\partial x^2} \frac{1}{\tau(x, s)}. \quad (6)$$

Since the left hand side just depends on r and the right hand side on x and s , they both have to be constant.

Solving the left hand side of (6) By denoting the constant $-\alpha^2 \lambda_r / \lambda_x$, one gets (Nagle et al., 1996)

$$\frac{\lambda_r}{\lambda_x} \frac{\partial^2 \psi(r)}{\partial r^2} \frac{1}{\psi(r)} + \frac{\lambda_r}{\lambda_x} \frac{\partial \psi(r)}{\partial r} \frac{1}{r} \frac{1}{\psi(r)} = -\frac{\lambda_r}{\lambda_x} \alpha^2,$$

or even:

$$r \frac{\partial^2 \psi(r)}{\partial r^2} + \frac{\partial \psi(r)}{\partial r} + \alpha^2 r \psi(r) = 0,$$

a well known form as the Bessel equation of order $\nu = 0$, which is a specific case of the Sturm-Liouville problem (Al-Gwaiz, 2008). The two solutions are the Bessel functions of first and second kinds. By superposition,

$$\psi(r) = K_1^* J_0(\alpha r) + K_2^* Y_0(\alpha r),$$

ψ must be continuous in $r = 0$, which implies that $K_2^* = 0$ from boundary condition (4). Since a linear superposition in θ will be taken, it can be considered that:

$$\psi(r) = J_0(\alpha r). \quad (7)$$

From last boundary condition (5), one gets

$$-\alpha \lambda_r J_1(\alpha R) + h_r J_0(\alpha R) = 0 \quad (8)$$

which has an infinity of solutions for any α . Since each associated function $\psi(r)$ will be orthogonal with respect to each other (linear independent given a specific inner product), the general solution will be the superposition of each associated θ function. Specifically, the inner product

$$\langle f_1(r), f_2(r) \rangle := \int_0^R r f_1(r) f_2(r) dr \quad (9)$$

is the one that results from this solution of the Bessel equation. If we use the subscript m to identify the solution for α_m , i.e., the m -th root of (8), then

$$\theta(x, r, s) = \sum_{m=0}^{\infty} c_m \tau_m(x, s) \psi_m(r).$$

Without loss of generality, it can be considered that

$$\frac{1}{c_m} = \mathcal{N}_m^2 := \int_0^R r \psi_m^2(r) dr,$$

where \mathcal{N}_m denotes the norm of $\psi_m(r)$ in the vector space defined with the inner product (9).

Using some properties of the Sturm-Liouville problem, by applying the inner product of the general solution with a n -th solution of the equation, one writes

$$\begin{aligned} \langle \theta(x, r, s), \psi_n(r) \rangle &= \int_0^R \theta(x, r, s) r \psi_n(r) dr \\ &= \sum_{m=0}^{\infty} c_m, \tau_m(x, s) \int_0^R r \psi_m(r) \psi_n(r) dr. \end{aligned} \quad (10)$$

Since the solutions are orthogonal, for every term with $m \neq n$ the integral will be equal to zero. Consequently, the only remaining terms are $n = m$:

$$\tau_m(x, s) = \int_0^R \theta(x, r, s) r \psi_m(r) dr.$$

Such an equation is an integral transform that rewrites the heat transfer problem in a new coordinate system given by $\psi_m(r)$ instead of r . The heat flux transform can be expressed by

$$\eta_m(x, s) := \int_0^R \varphi(x, r, s) r \psi_m(r) dr.$$

Considering that the heat flux will be applied in the center of the thermocouple, and by substituting in the last equation it is easy to see that

$$\eta_m(0, s) = \varphi(0, r, s) \int_0^{R_0} r \psi_m(r) dr. \quad (11)$$

Solving the right hand side of (6) By rewriting (6), one writes

$$\frac{\partial^2 \tau_m}{\partial x^2} = \left(\frac{s}{a_x} + \alpha_m^2 \frac{\lambda_r}{\lambda_x} \right) \tau_m.$$

The solution is defined as

$$\tau_m(x, s) = K_1 \cosh(k_m \ell) + K_2 \sinh(k_m \ell),$$

where the constant k_m in 2D is expressed as

$$k_m = \sqrt{\frac{s}{a_x} + \alpha_m^2 \frac{\lambda_r}{\lambda_x}}.$$

The goal being to establish a relation between the temperature at the rear $\tau_m(\ell, s)$ and the heat flux at the front $\eta_m(0, s)$, the thermal transfer function $G_\varphi^m(s)$ is explicitly defined by

$$G_\varphi^m(s) = \frac{\tau_m(\ell, s)}{\eta_m(0, s)} = \frac{1}{\lambda_x k_m \sinh(\ell k_m) + h_x \cosh(\ell k_m)}. \quad (12)$$

Unfortunately, the general transfer function $G_\varphi(s)$ cannot be taken as a direct series of $G_\varphi^m(s)$. It will be considered the transfer function of interest is about the heat flux in the x direction that is been measured in the middle of the thermocouple $\phi(0, r, t)$ for $r < R_0$:

$$G_\varphi(s) = \frac{\theta(\ell, 0, s)}{\varphi(0, r, s)} = \sum_{m=0}^{\infty} \frac{\tau_m(\ell, s)}{\varphi(0, r, s)} \frac{\psi_m(0)}{\mathcal{N}_m^2}.$$

or else

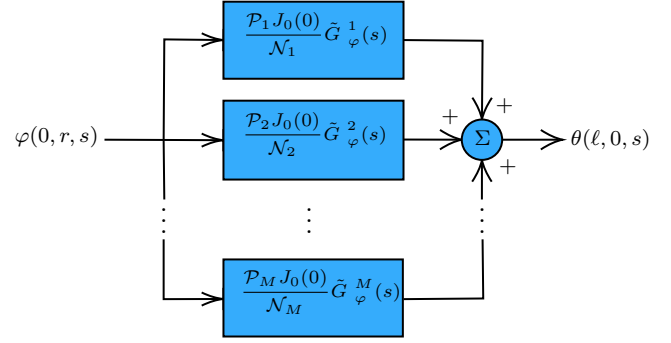


Fig. 3. 2D heat transfer block diagram

$$G_\varphi(s) = \sum_{m=0}^{\infty} \frac{G_\varphi^m(s) \eta_m(0, s) \psi_m(0)}{\varphi(0, r, s) \mathcal{N}_m^2}.$$

Using relation (11), it is possible to write

$$G_\varphi(s) = \sum_{m=0}^{\infty} G_\varphi^n(s) \frac{\mathcal{P}_m \psi_m(0)}{\mathcal{N}_m^2},$$

with

$$\mathcal{P}_m := \int_0^{R_0} r \psi_m(r) dr.$$

Finally, by truncating the sum at M , the final two-dimensional solution is expressed by

$$G_\varphi(s) = \sum_{m=0}^M \frac{\mathcal{P}_m J_0(0)}{\mathcal{N}_m^2} \frac{1}{\lambda_x k_m \sinh(\ell k_m) + h_x \cosh(\ell k_m)}. \quad (13)$$

which is a complex function of s . Fig. 3 gives a block diagram to help the simulation of such a transfer function for a given sum of M terms.

Fig. 4 and Fig. 5 show the analytical model (in black plain line) developed from equation (13), with $h_x = h_r = 17$.

3. 2D HEAT TRANSFER APPROXIMATIONS

The transfer function (13) is difficult to use in practice, and finding its inverse is a non trivial task. In order to invert it, a polynomial approximation is used. There are some possibilities and the most common one is by using the Taylor series expansion. Rewriting (13) by replacing explicitly sinh and cosh with their Euler form and using a new variable $\xi_m = \ell k_m$, one gets

$$G_\varphi(\xi_m) = \sum_{m=0}^M \frac{\mathcal{P}_m J_0(0)}{\mathcal{N}_m^2} \frac{1}{A(\xi_m) e^{\xi_m} + B(\xi_m) e^{-\xi_m}}, \quad (14)$$

with

$$\begin{cases} A(\xi_m) = \frac{\lambda_x \xi_m + h_x}{2\ell} \\ B(\xi_m) = -\frac{\lambda_x \xi_m + h_x}{2\ell} \end{cases}$$

3.1 Taylor approximation

The Taylor series approximation will be applied to the exponential term, by taking

$$e^{\xi_m} = \frac{e^{\xi_m/2}}{e^{-\xi_m/2}} \approx \frac{\sum_{i=0}^N \xi_m^i / i!}{\sum_{j=0}^N (-1)^j \xi_m^j / j!} = \frac{P(\xi_m)}{Q(\xi_m)}. \quad (15)$$

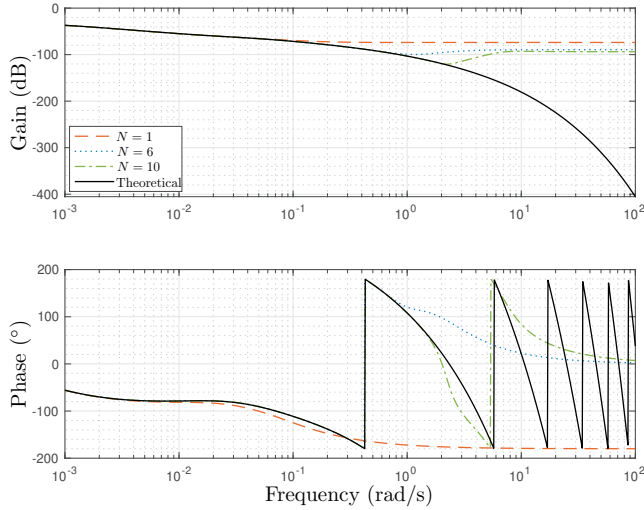


Fig. 4. Taylor approximations for different values of N with $h_x = h_r = 17$ and $M = 6$

Table 1. Parameters for the 1D thermal system

Variable	Name	Value	Unit
λ	Thermal conductivity	15	W/m.K
ρ	Density	7900	kg/m ³
c_p	Specific heat	500	J/kg.K
ℓ	Thermocouple depth	10	mm

The approximated Taylor transfer function $\tilde{G}_\varphi^T(\xi_m)$ can then be expressed by

$$\begin{aligned} \tilde{G}_\varphi^T(\xi_m) &= \sum_{m=0}^M \frac{\mathcal{P}_m J_0(0)}{\mathcal{N}_m^2} \frac{1}{A(\xi_m) \frac{P(\xi_m)}{Q(\xi_m)} + B(\xi_m) \frac{Q(\xi_m)}{P(\xi_m)}} \\ &= \sum_{m=0}^M \frac{\mathcal{P}_m J_0(0)}{\mathcal{N}_m^2} \frac{P(\xi_m) Q(\xi_m)}{A(\xi_m) P(\xi_m) P(\xi_m) + B(\xi_m) Q(\xi_m) Q(\xi_m)}. \end{aligned} \quad (16)$$

From the parameters given in Table 1, Fig. 4 shows the Bode diagrams of the analytical G_φ expression and its Taylor approximations \tilde{G}_φ^T using different values of N .

It can clearly be seen that the higher N is, the wider the frequency range validity is. However, increasing significantly N will not significantly enlarge the frequency band of the Taylor approximation. For example, with $N = 10$, the approximation validity is limited to 2 rad/s.

3.2 Padé approximation

Though the Taylor approximation for $e^{\pm\xi_m/2}$ gives satisfactory results, the approximation can be better by using a Padé approximation for any indeterminate ξ_m :

$$e^{\xi_m} = \frac{P'(\xi_m)}{Q'(\xi_m)} + o(\xi^{2N+1}), \quad (17)$$

with

$$\begin{aligned} P'(\xi) &= \sum_{i=0}^N \frac{(2N-i)! N! \xi^i}{2N!(N-i)! i!} \\ Q'(\xi) &= \sum_{i=0}^N \frac{(2N-i)! N! (-\xi)^i}{2N!(N-i)! i!}. \end{aligned}$$

The denominator and numerator degree should not necessarily be the same, however, by doing so, we have $P(-\xi) =$

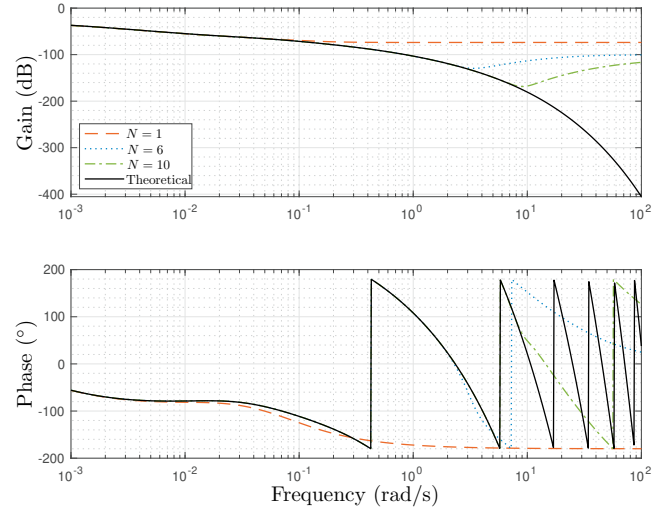


Fig. 5. Padé approximations for different values of N with $h_x = h_r = 17$ and $M = 6$

$Q(\xi)$. Thus, the Padé approximated function \tilde{G}_φ^P is expressed by

$$\tilde{G}_\varphi^P(\xi) = \sum_{m=0}^M \frac{\mathcal{P}_m J_0(0)}{\mathcal{N}_m^2} \frac{P'(\xi_m) Q'(\xi_m)}{A(\xi_m) P'(\xi_m) P'(\xi_m) + B(\xi_m) Q'(\xi_m) Q'(\xi_m)}. \quad (18)$$

From the parameters given in Table 1, Figure 5 shows the Bode diagrams of the analytical G_φ expression and its Padé approximations using different values of N .

Again, the higher N is, the wider the approximation frequency range is. The frequency range of the Padé approximation is even larger than with the Taylor approximation. For example, with $N = 10$, the frequency range validity of the Padé approximation goes up to 9 rad/s. Given the experimental section 4.1, the bandwidth is around 3 rad/s.

3.3 Finite difference modeling

For the numerical method, the Crank-Nicolson method is used in a two-dimensional analysis. Figs. 6 and 7 shows the mesh and the phantom-nodes that were created. Note that, not only the two boundary conditions for each variable have to be analyzed, but also the equation for a node that is simultaneously in both boundary conditions (node at the mesh corner).

By writing the approximations and denoting $T_{i,j}^n = T(x_j, r_i, t_n)$, one can write

$$\begin{aligned} \frac{\partial T}{\partial t} &\approx \frac{T_{i,j}^{n+1} - T_{i,j}^n}{\Delta t}, \\ \frac{\partial T}{\partial r} &\approx \frac{-T_{i,j-1}^n - T_{i,j-1}^{n+1} + T_{i,j+1}^n + T_{i,j+1}^{n+1}}{2\Delta r}, \\ \frac{\partial^2 T}{\partial r^2} &\approx \frac{T_{i,j-1}^n + T_{i,j-1}^{n+1} - 2(T_{i,j}^n + T_{i,j}^{n+1}) + T_{i,j+1}^n + T_{i,j+1}^{n+1}}{2\Delta r^2}, \\ \frac{\partial^2 T}{\partial x^2} &\approx \frac{T_{i-1,j}^n + T_{i-1,j}^{n+1} - 2(T_{i,j}^n + T_{i,j}^{n+1}) + T_{i+1,j}^n + T_{i+1,j}^{n+1}}{2\Delta x^2}. \end{aligned}$$

Replacing these expressions in (1), one gets

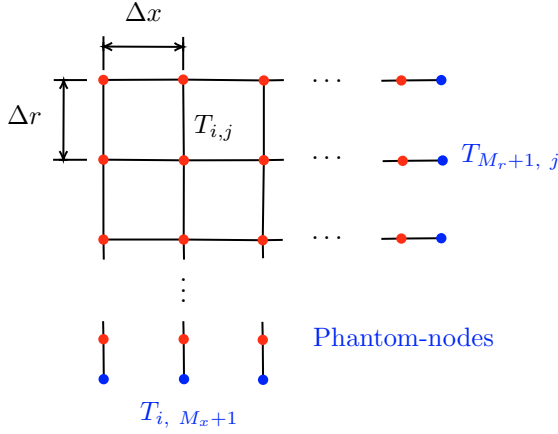


Fig. 6. Mesh for finite difference

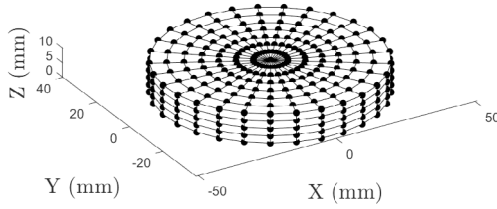


Fig. 7. Mesh built with Matlab

$$\begin{aligned}
 (\sigma_2 - \sigma_1)T_{i-1,j}^{n+1} + (2 + 2\sigma_1 + 2\sigma_3)T_{i,j}^{n+1} + (-\sigma_1 - \sigma_2)T_{i+1,j}^{n+1} \\
 + (-\sigma_3)T_{i,j-1}^{n+1} + (-\sigma_3)T_{i,j+1}^{n+1} = (\sigma_1 - \sigma_2)T_{i-1,j}^n + \\
 (2 - 2\sigma_1 - 2\sigma_3)T_{i,j}^n + (\sigma_1 + \sigma_2)T_{i+1,j}^n + (\sigma_3)T_{i,j-1}^n + (\sigma_3)T_{i,j+1}^n
 \end{aligned}$$

with $\sigma_1 = a_x \Delta t / \Delta r^2$, $\sigma_2 = a_x \Delta t / r \Delta r$ and $\sigma_3 = a_x \Delta t / \Delta x^2$, Δx the simulation time step, $M_x = \ell / (\Delta x) + 1$ and $M_r = R / (\Delta r) + 1$ the number of nodes in the x and r directions, respectively.

By introducing phantom nodes at the end points, new equations can be derived to include the boundary conditions. At the rear surface ($x = \ell$) for $r \neq R$, one gets

$$T_{i, M_x+1}^n = \frac{2h_x \Delta x}{\lambda_x} T_{i, M_x}^n + T_{i, M_x-1}^n,$$

which gives,

$$\begin{aligned}
 (\sigma_2 - \sigma_1)T_{i-1,j}^{n+1} + \left(2 + 2\sigma_1 + 2\sigma_3 + \frac{2h_x \Delta x}{\lambda_x}\right) T_{i,j}^{n+1} \\
 + (-\sigma_1 - \sigma_2)T_{i+1,j}^{n+1} + (-2\sigma_3)T_{i,j-1}^{n+1} = (\sigma_1 - \sigma_2)T_{i-1,j}^n \\
 + \left(2 - 2\sigma_1 - 2\sigma_3 - \frac{2h_x \Delta x}{\lambda_x}\right) T_{i,j}^n + (\sigma_1 + \sigma_2)T_{i+1,j}^n + (2\sigma_3)T_{i,j-1}^n.
 \end{aligned}$$

From the boundary conditions (2)–(5), a complete matrix expression is built:

$$\mathbf{R}\mathbf{T}^{n+1} - \mathbf{c}^{n+1} = \mathbf{S}\mathbf{T}^n + \mathbf{c}^n, \quad (20)$$

where the temperature vector for all nodes at a time t_n is given by

$$\mathbf{T}^n = \begin{pmatrix} T_1^n \\ T_2^n \\ \vdots \\ T_{M_x}^n \end{pmatrix} = \begin{pmatrix} T_{1,1}^n \\ \vdots \\ T_{M_r,1}^n \\ T_{1,2}^n \\ \vdots \\ T_{M_r,2}^n \\ \vdots \\ T_{M_r, M_x}^n \end{pmatrix}. \quad (21)$$

and

$$\mathbf{c}^n = \begin{pmatrix} \frac{2h_x \Delta x \sigma}{\lambda_x} \phi(0, r, t_n) \\ 0 \\ \vdots \\ 0 \end{pmatrix},$$

and the matrices \mathbf{R} and \mathbf{S} have much more complicated forms and cannot be easily shown. The higher the mesh size, the better the precision. Here, it is sufficiently high to guarantee precision and convergence of the solution.

4. BENCHMARK AND EXPERIMENT VALIDATION

4.1 Benchmark description

The whole benchmark configuration is described on Fig. 8. The thermal system is composed of a (stainless steel) sample that constitutes the lower surface of a space shuttle which is provided by the ONERA (French Aerospace Lab). The sample is a cylinder of depth 15mm and of diameter 80mm. A thermocouple (K-type) is stucked at the center of the rear surface. A heating resistor is put at the front the shuttle sample and has the same diameter (to ensure one dimensional diffusion); consequently, the heat flux is produced by the heating resistor which is supplied by a controllable/programmable voltage source (EA-PSI 9000-2U). The whole data acquisition is carried out by a portable recorder (DAS 240BAT) that gets a maximal sampling rate of 1ms.

A Labview program was developed to get a controllable experimental setup and was implemented to communicate with both the voltage source and the DAS 240.

To avoid irregular time acquisition data by the computer, even if the Labview program reads and shows the data for online structural health monitoring (SHM), the final data is obtained by taking the recorded REC files in the DAS. The file transfer is done via FFT protocol and converted to TXT files, which can be easily read by Matlab®.

The Labview program was developed in order to apply a pseudo random binary signal (PRBS) to the thermal system, offering an input that is persistently exciting in the frequency range of interest. In the experiment, the input is a set between $[0, 14.2] W.m^{-2}$. The sampling time is set to $T_s = 0.1s$.

4.2 Comparison with the model approximations

Fig. 9 compares the experimental temperature output results with a 2-dimensional simulation (the heat transfer has been set to $h = 20$ after a steady state study, which is usually in $[5, 25]$) obtained with the Taylor expansion approximation, Padé expansion approximation and a finite difference method.

The approximation results tend to be considerably smaller than the true experimental output. Such an experiment shows the need for system identification of the true system as the approximated models stemming from the analytical model do not take into account the true conduction diffusion/loss exchanges in the benchmark. On the contrary, the three approximation models have exactly the same behavior. Since the heat shield and materials are normally not homogeneous, a pure analytical model of $G_\varphi(q^{-1})$ is not appropriate: system identification is required.

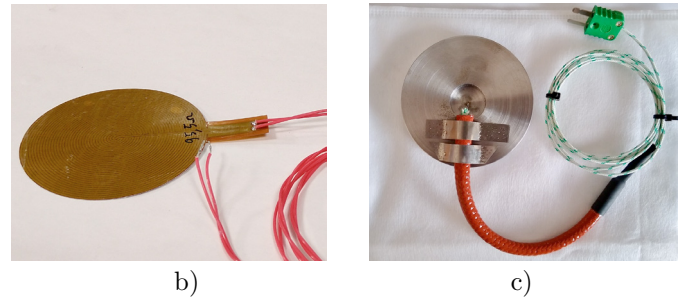
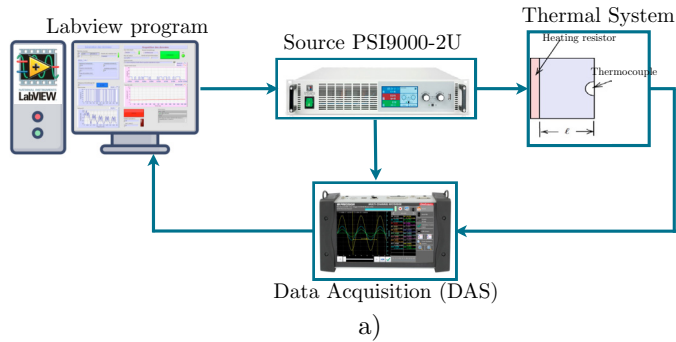


Fig. 8. Benchmark configuration: a) experimental setup; b) heating resistor; c) stainless steel sample with thermocouple

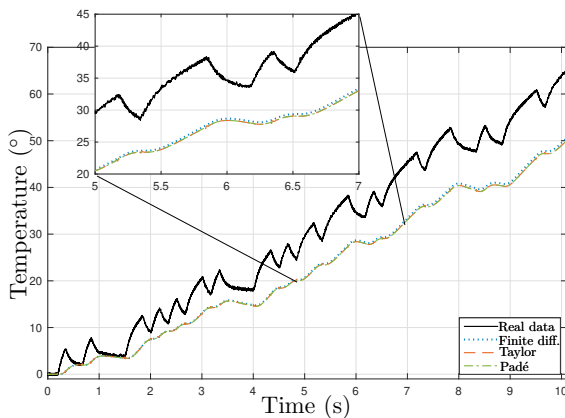


Fig. 9. Comparison of the true output with 2D model approximations

5. CONCLUSION

The proposed models should be easily invertible in order to reconstruct the heat flux in atmosphere reentry. The theoretical and thermal approximation models have shown their limit when considering experimental data. All the presented numerical approximations lack of precision: the finite difference method seems to be more precise, however it will not be possible to reconstruct the input heat flux; the Padé and Taylor approximations are also far from the true output temperature. This study clearly shows that an optimized estimation of the thermal transfer function is necessary by considering the heat transfer coefficient, loss factor and the true material properties. For future works, system identification should be carried out in order to get the true system physical parameters and by considering more complex model structures.

6. ACKNOWLEDGEMENTS

This study received financial support from the French government in the framework of the France 2030 program for University of Bordeaux / RRI BEST (french acronym for Research Network on Factory of the future). Moreover, the authors would like to thank the ONERA (French Aerospace Lab) for providing us a stainless steel sample with a stucked thermocouple.

This study was financed in part by the Coordenação de Aperfeiçoamento de Pessoal de Nível Superior - Brasil (CAPES) - Finance Code 001.

REFERENCES

Al-Gwaiz, M. (2008). *Sturm-Liouville Theory and its Applications*. Springer-Verlag London.

- Anderson, J. (1989). *Hypersonic and high temperature gas dynamics*. McGraw-Hill.
- Chinen, K., Kinjo, I., Zamami, A., Irei, K., and Nagayama, K. (2015). New equivalent-electrical circuit model and a practical measurement method for human body impedance. *Bio-Medical Materials and Engineering*, 26, S779–S786. doi:10.3233/BME-151369.
- Danza, L., Belussi, L., Meroni, I., Salamone, F., Floreani, F., Piccinini, A., and Dabusti, A. (2016). A simplified thermal model to control the energy fluxes and to improve the performance of buildings. *Energy Procedia*, 101, 97 – 104. doi:10.1016/j.egypro.2016.11.013.
- Duhé, J., Victor, S., Melchior, P., Abdelmoumen, Y., and Roubertie, F. (2022). Modeling thermal systems with fractional models: human bronchus application. *Nonlinear Dynamics*, 108, 579–595. doi:10.1007/s11071-022-07239-3.
- Ismail, N., Ghaddar, N., and Ghali, K. (2018). Electric circuit analogy of heat losses of clothed walking human body in windy environment. *International Journal of Thermal Sciences*, 127, 105 – 116. doi:https://doi.org/10.1016/j.ijthermalsci.2018.01.025.
- Kemp, N. and Riddell, F. (1957). Heat transfer to satellite vehicles re-entering the atmosphere. *Journal of Jet Propulsion*, 27(2), 132–137. doi:10.2514/8.12603.
- Künzi, R. (2015). Thermal design of power electronic circuits. *arXiv: Accelerator Physics*, 3, 311–327. doi:10.5170/CERN-2015-003.311.
- Maillet, D., André, S., Batsale, J., Degiovanni, A., and Moyne, C. (2000). *Thermal Quadrupoles: Solving the Heat Equation through Integral Transforms*. Loyola Symposium Series. John Wiley & Sons.
- Nagle, R.K., Saff, E.B., Snider, A.D., and West, B. (1996). *Fundamentals of differential equations and boundary value problems*. Addison-Wesley New York.
- Parnis, G. (2012). Building thermal modelling using electric circuit simulation. URL <http://handle.unsw.edu.au/1959.4/51971>.
- Pizzarelli, M., Boehrk, H., Weihs, H., and Elsäßer, H. (2019). Hot structure flight data of a faceted atmospheric reentry thermal protection system. *International Journal of Aerospace Engineering*, 9754739. doi:10.1155/2019/9754739.
- Zhang, L., Peng, H., Ning, Z., Mu, Z., and Sun, C. (2017). Comparative research on RC equivalent circuit models for lithium-ion batteries of electric vehicles. *Applied Sciences*, 7(10). doi:10.3390/app7101002.